Quaternary Science Advances 15 (2024) 100207

Contents lists available at ScienceDirect

Quaternary Science Advances

journal homepage: www.sciencedirect.com/journal/quaternary-science-advances

Development of an automated extraction and radiocarbon dating method for fossil pollen deposited in lake Motosu, Japan

Kosuke Ota [a,b,c,*], Yusuke Yokoyama [a,b,d,e,f,**], Yosuke Miyairi [a], Stephen P. Obrochta [g], Shinya Yamamoto [h], A. Hubert-Ferrari [i], V.M.A. Heyvaert [j,k], Marc De Batist [k], Osamu Fujiwara [c], the QuakeRecNankai Team

[a] Atmosphere and Ocean Research Institute, The University of Tokyo, Chiba, Japan
[b] Department of Earth and Planetary Science, The University of Tokyo, Tokyo, Japan
[c] Geological Survey of Japan, National Institute of Advanced Industrial Science and Technology, Ibaraki, Japan
[d] Graduate Program on Environmental Sciences, Graduate School of Arts and Sciences, The University of Tokyo, Tokyo, Japan
[e] Biogeochemistry Program, Japan Agency for Marine-Earth Science and Technology, Kanagawa, Japan
[f] Research School of Physics, The Australian National University, Canberra, Australia
[g] Graduate School of International Resource Science, Akita University, Akita, Japan
[h] Mount Fuji Research Institute, Yamanashi Prefectural Government, Yamanashi, Japan
[i] University of Liege Department of Geography, Belgium
[j] Geological Survey of Belgium, Royal Belgian Institute of Natural Sciences, Belgium
[k] Ghent University Department of Geology, Belgium

A B S T R A C T

Recently, radiocarbon (^{14}C) dating methods using fossil pollen extracted from sediments with a flow cytometer (cell sorter) are under development. Technical limitations experienced by previous studies required extraction of grains <80 μm in diameter. Thus, obtaining a sufficient mass of carbon for dating requires extracting a very large number (~10^5) of grains. Another challenge faced by earlier work was preventing contamination by exotic carbon during the extraction process. Here we present a novel solution to this problem by using a cell sorter with a newly designed pretreatment method and an improved extraction method. This enables us to extract large pollen fossils than was previously possible. By using grains, >100 μm in diameter, such as *Pinus* sp., we have reduced the number of grains for required for ^{14}C dating by an order of magnitude, particularly when considering the recent advances in measure ultra-small carbon masses on a single-stage accelerator mass spectrometer at the Atmosphere and Ocean Research Institute, University of Tokyo. We then apply this method to sediments recovered from Lake Motosu, which already has a very robust chronology, to evaluate the new method. Results indicate the method is successful and reveal temporal radiocarbon reservoir effects that appear related to the changes in the depositional environment and/or hydroclimate. The method presented here is widely applicable across multiple environments.

1. Introduction

Reconstructing paleoenvironments from sedimentary archives requires the development of a reliable chronology. Lacustrine sediments are of particular interest because they can represent high-resolution archives of past regional environmental and climatic changes, often with minimal complicating factors that are common to marine archives. Radiocarbon (^{14}C) dating is one of the most widely used methods for dating lacustrine sediments and is applicable over the past 55,000 years. However, lacustrine sediment may contain a mixture of older, reworked terrestrial organic matter and newer, aquatically produced organic matter, causing dates on bulk organic matter to be older than the actual age of deposition (Philippsen, 2013; Nakamura et al., 2016). Also, similar to the oceans, lakes may be subject to a carbon reservoir effect due to the presence of old, dissolved carbon. Thus, even in the absence of reworked terrestrial organic matter, aquatic organic matter radiocarbon ages may still be older than the age of production (Obrochta et al., 2018; Ota et al., 2021, 2023; Yamamoto et al., 2023). The most common cause of the carbon reservoir effect is the dissolution of ^{14}C-depleted carbon into lake waters and its subsequent uptake by aquatic plants and organisms (Howarth et al., 2013; Zhang et al., 2021). This carbon typically originates from the migration of aged terrestrial organic carbon (OC)

* Corresponding author. Atmosphere and Ocean Research Institute, The University of Tokyo, Chiba, Japan.
** Corresponding author. Atmosphere and Ocean Research Institute, The University of Tokyo, Chiba, Japan.
E-mail addresses: k.ota@aist.go.jp (K. Ota), yokoyama@aori.u-tokyo.ac.jp (Y. Yokoyama).

https://doi.org/10.1016/j.qsa.2024.100207
Received 13 March 2024; Received in revised form 6 June 2024; Accepted 7 June 2024
Available online 11 June 2024

and catchment carbonates (Hou et al., 2012). Generally, age models for such lakes are established by assessing the current carbon reservoir effect and modifying the chronology based on ^{14}C dating of total organic carbon (TOC; Geyh et al., 1997).

Intact terrestrial plant macrofossils deposited parallel to the bedding plane are traditionally considered the most suitable material for accurate ^{14}C dating, not only because they fix carbon directly from, and in equilibrium with, atmospheric CO_2 (Bertrand et al., 2012), but also because their excellent preservation indicates (geologically) immediate deposition in the lake. Therefore, terrestrial plant macrofossils are unaffected by any potential lake reservoir effect, but their presence is sporadic. In oxidative benthic environments, terrestrial plant leaves and wood fragments often decompose quickly after deposition, and even in anoxic conditions, deposition of terrestrial plant macrofossils is not continuous. Thus, TOC is often the only material available for ^{14}C dating.

^{14}C dating of fossil pollen collected from sediments has been developed to provide atmospheric radiocarbon ages for intervals devoid of terrestrial plant macrofossils. One reason is that developments in accelerator mass spectrometry (AMS) over the past 30 years have greatly reduced the sample size required to obtain reliable ^{14}C ages to <100 μg carbon (Yokoyama et al., 2010, 2022; Hua et al., 2001; Shah and Pearson, 2007). Separation of individual pollen has traditionally been done by microscopic collection or chemical treatment alone (Brown et al., 1989; Fletcher et al., 2017), but this procedure often results in suboptimal pollen purity. Flow cytometers (cell sorters) are being used to separate pollen in sufficient quantities and with the required high purity (Kasai et al., 2021; Omori et al., 2023; Steinhoff et al., 2022; Tennant et al., 2013; Yamada et al., 2021; Zimmerman et al., 2019). Collecting and dating of fossil pollen by flow cytometry was first achieved with physical and chemical pre-treatment (Tennant et al., 2013). In parallel with the refinement of the operating protocol, cell sorter technology has also improved. Until recently, only small pollen grains (<80 μm in diameter) could be extracted (e.g., Tunno et al., 2021; Yamada et al., 2021). However, the method is currently in the early stages of development.

The initial, pioneering studies on ^{14}C dating of fossil pollen collected by cell sorters have shown the technique to be generally reliable, but pollen ages may deviate from those of large fossil leaves by many hundreds of years. Possible reasons for such discrepancies include lack of purity of the pollen and modern CO_2 contamination during the pretreatment process. Although there were examples of studies that had a high agreement with large fossils, the sample size available for the cell sorter was limited (e.g., Tunno et al., 2021; Yamada et al., 2021). Thus, further improvement of the extraction method is needed.

Here, we present a comprehensive, easily implementable flow cytometry method for pollen extraction using pre-treatment of trace organic matter samples with little to no modern carbon contamination. We demonstrate the method on sediments recovered from Lake Motosu, Japan, to evaluate temporal variability in the carbon reservoir effect.

2. Geological setting

Lake Motosu is located on the northwest side of Mount Fuji and has a maximum depth of 121.1 m and an average depth of 67.9 m (Fig. 1). The south, west, and north sides of Lake Motosu consist of sedimentary rocks and volcaniclastic debris (pyroclastic and basaltic lava, mudstone, sandstone, dacite, and tuff) of the Furusekisawa and Tokiwa formations (Takada et al., 2013), while the east and southeast sides are catchments composed of younger volcanic products (Hamada et al., 2012). Lake Motosu has no continuous river input, and groundwater contributes to the lake. The eastern side of the present lake is covered with gently sloping terrain formed by the Aokigahara lava flow, which is porous and extremely permeable (Takada et al., 2016). Detailed measurements of sediments and lake water have been obtained for current carbon reservoir ages (R), yielding ^{14}C ages for dissolved inorganic carbon in the surface waters of about 222 ± 70 BP (Before Present, relative to 1950), and dissolved inorganic carbon is thought to be incorporated into the sediments through summer photosynthesis (Obrochta et al., 2018; Ota et al., 2021, 2023).

Located to the northwest of Mt. Fuji, Lake Motosu is relatively shielded from eruptions because of the prevailing westerly winds. Yet, several pyroclastic events have been reported such as the Omuroyama eruption (3056–3260 cal BP; Yamamoto et al., 2005) that formed a large scoria cone near the lake. At minimum three lava flows (i.e. Motosu lava flow, Lake Motosu lava flow, and Aokigahara lava flow) have impacted the lake. Core drilling taken along the eastern margin of the lake indicates that approximately 21.4 m of lava was deposited during the Motosu lava flow, the Lake Motosu lava flow and the last lava flow was the CE 864 Aokigahara lava flow (Koshimizu et al., 2007).

Only two of a total of more than 14 scoria fall deposits reported for the Subashiri-b phase (5.6–3.5 cal kBP) (Miyaji, 1988) have been detected in the vicinity of Lake Motosu. Along the western flank of the mountain, the remains of 4 pyroclastic density flows are present. These include the SYP1 and 2, reported as 3384–3561 cal BP and 3140–3356 cal BP, respectively, during which the Osawa scoria (Sc-Osw) was deposited (3214–3401 cal BP) (Yamamoto et al., 2005). Subsequent eruptions in the northwestern foothills formed the Omuro scoria fall deposit (Sc-Omr; 3072–3272 cal BP), followed by the deposition of SPY3 and SPY4 (2864–3078 and 2678–2754 cal BP). The last summit eruption

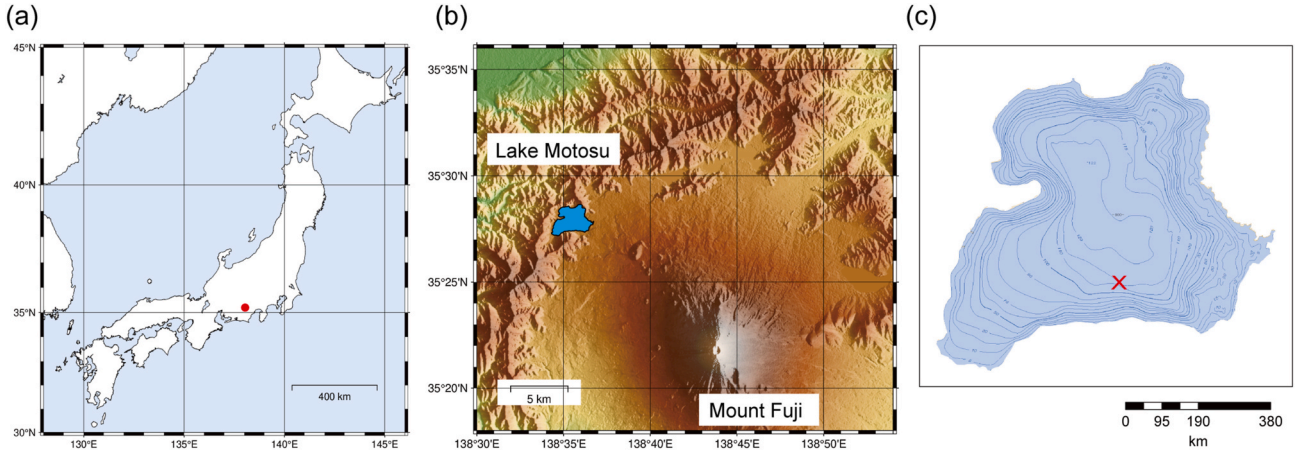

Fig. 1. (a) Geographic map of Japan. Red dot indicates region shown in panel (b). (b) Elevation map of the Mount Fuji region. (c) Lake Motosu is shown with bathymetry survey data collected in 2021 by the Geospatial Information Authority of Japan. The Contour interval is 5 m. Red cross shows the location of site MOT-15-2.

(Kenganmine; Sc-Kng) occurred at the end of the Subashiri-c phase (3500–2300 cal BP) (Yamamoto et al., 2005). Obrochta et al. (2018) reported two previously unknown eruptions, likely of relatively small magnitude, that occurred ~20 years apart between ~ 2292 and 2616 cal BP.

3. Materials and methods

3.1. Core samples and stratigraphy

We analyzed a continuous 3.67 m composite sediment section spliced from multiple piston cores recovered at site MOT-15-2, near the deepest part of Motosu Lake (Obrochta et al., 2018).

The core is composed mainly of a mixture of siliceous biogenic and fine clastic particles with wide-spread tephra layers (Kawagodaira; Kg, Kikai Akahoya; K-Ah) identified by micro X-ray CT, μXRF, and EPMA analysis. ^{14}C dating of fossil leaves and bulk sediments was also performed (Obrochta et al., 2018). Five scoria layers after the Kg tephra fallout (3149 ± 12 cal BP; Tani et al., 2013) were reported from the site MOT-15-2 cores, providing insight into multiple Mount Fuji eruptions that were not well distinguished on land where erosion is predominant. The scoria-fall layers recovered at MOT-15-2 correspond to Osawa (2829–3093 cal BP), Omuro (2767–3053 cal BP), two undetected eruptions (2292–2643 and 2272–2616 cal BP), and the Kengamine eruptions (2119–2453 cal BP) (Obrochta et al., 2018).

3.2. Physical and chemical pre-treatment

While a cell sorter can identify fluorescent properties of materials, sorting samples that contain many impurities is time consuming. In addition, needle-like impurities may have a long axis that exceeds the diameter of the flow path, potentially causing clogging. Therefore, appropriate physical and chemical pretreatment is necessary to selectively remove impurities such as lithic material and plant fragments. Here we introduce an efficient physical and chemical pretreatment method appropriate for the extraction of large fossil pollen up to 150 μm in diameter.

The pretreatment protocol is illustrated in Fig. 2. To remove and deflocculate organic matter such as humic acid, 10 wt% KOH is added to 10–20 g of sample that is then heated to 70 °C for 30 min to 2 h until the humic acid is eluted. After cooling, the sample is washed twice with ultra-pure water. After washing, the sample is passed through a 2-mm mesh to separate the large mineral fraction and then mixed with a high-density $ZnCl_2$ solution and centrifuged at 1000 rpm for 25 min and at 1200 rpm for a further 5 min. The solution density is 2.15 g/ml, which is optimal for recovery of fossil pollen (Morita, 2012). The $ZnCl_2$ solution is removed by mixing the supernatant solution containing pollen with 10 wt% HCl and washing twice with ultra-pure water. The sample is then reacted at room temperature for 30 min with a 50 wt% HF solution to remove diatoms and other non-organic matter. After washing twice with ultra-pure water, the final step is to remove needle-like organic matter by sieving with a 140 μm sieve. This procedure allowed for processing four to eight samples per person per day.

3.3. On-chip sorting

We used an "On-Chip Sort" microfluidic chip-based cell sorter produced by On-Chip Biotechnologies Co., Ltd. of Tokyo, Japan, coupled to a disposable sample line to facilitate faster line replacement when clogging occurs due to impurities (Fig. 3c). Ultra-pure water, free of organic materials, was used as the sheath liquid (carrier of sample). All particles were detected by multiple laser beams with wavelengths of 405, 488, and 561 nm. Detected particles are referred to as "events". The On-Chip Sort can measure particle fluorescence intensity, forward scatter channel (FSC; indicator of particle size), and side scatter channel (SSC; indicator of internal structure complexity) using six separate detectors (FL1 – FL6). Detector wavelength ranges are 445 ± 20 nm (FL1), 543 ± 22 nm (FL2), 591.5 ± 43 nm (FL3), 676 ± 37 nm (FL4), 716 ± 40 nm (FL5) and 775 ± 46 nm (FL6).

The detected particles are displayed in real-time as a two-dimensional scatterplot with selectable parameters for each axis. (Fig. 3a). This highlights particles with different optical properties. A region of the plot may be defined for more detailed investigation (Fig. 3b), and if the particles that are likely pollen are collected in the sample reservoir. In this study, the regions were defined by assuming that the samples with higher fluorescence intensity and larger particle size were pollen grains.

3.4. Elemental analyzer (EA)

After sorting, the fossil pollen were dried in silver cups treated with a methanol-acetone to remove an oil from cups that could cause contamination. Dry sample weight was recorded. The CO_2 gas was extracted with a Vario MICRO cube fully automated EA (Elemental

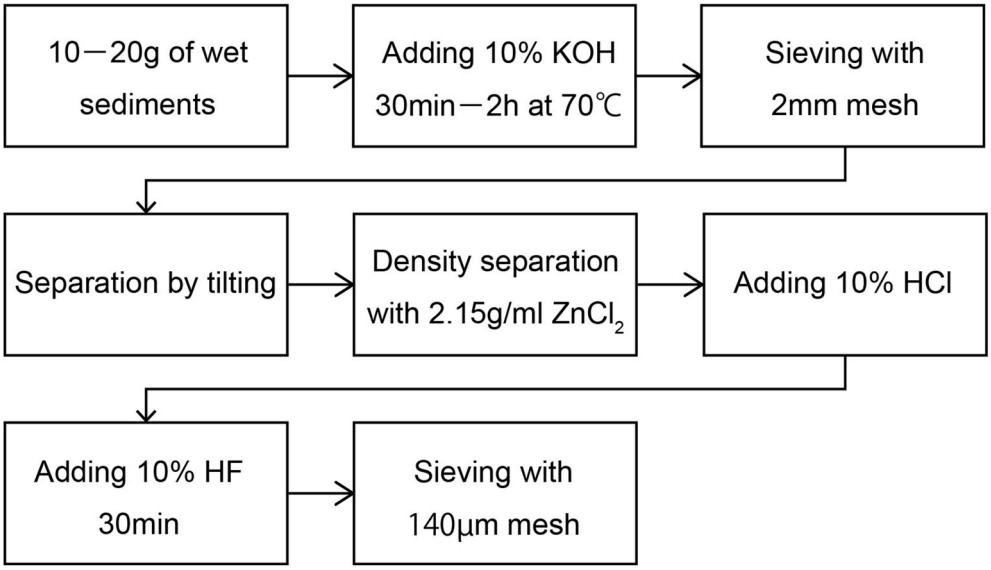

Fig. 2. Flowchart of pretreatment for large-size fossil pollen.

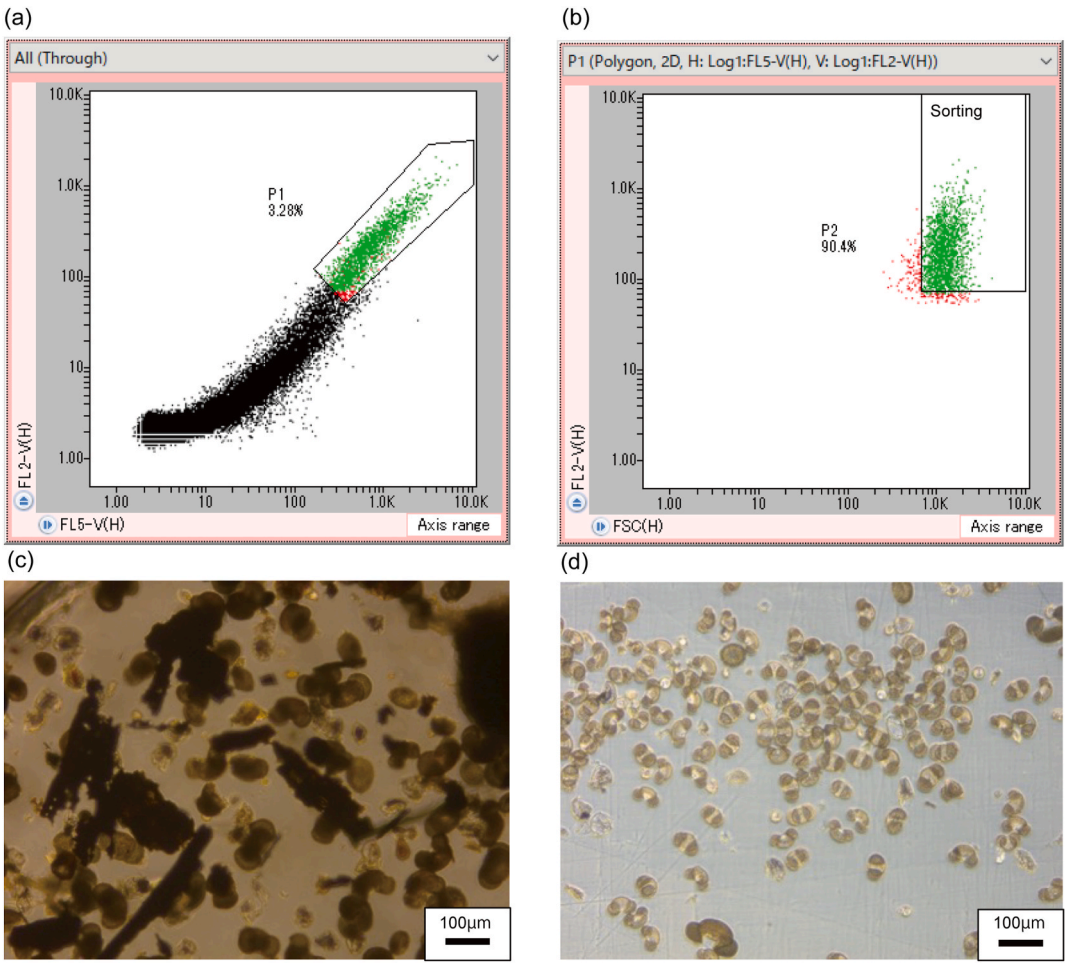

Fig. 3. (a) Fluorescence intensity of particles within core MOT-15-2 sampled at 1.7–1.72 mcd measured using a cell sorter after pretreatment. The color of markers reflects the selection of particles. Channel FL5 is plotted on the horizontal axis and FL2 on the vertical. Box denotes area P1, which contains 3.28% of the measured particles (b) Plot of FSC versus channel FL2 for particles in region P1. Pollen grains are concentration in the region defined as P2 (90.4% of region P1). Particles in region P2 are collected in the sample reservoir and shown in panel d. (c) Photomicrograph of this sample after pre-treatment but before sorting. (d) Photomicrograph of the sorted sample (particles in region P2).

Analysis, DKSH Japan, Inc.; Yokoyama et al., 2022), and carbon concentrations were measured. This enabled the removal of the non-carbon gas (nitrogen and sulfur gases) from the samples and efficient graphitization. Three age determinations (YAUT-063509, 063511, and 065119), were performed prior to the introduction of the EA, and their carbon concentrations were determined by loss on ignition (Table 1).

3.5. AMS measurements

The sample CO_2 was mixed with twice as much pure H_2 gas and introduced into a reaction vessel in which approximately 4.0 mg of Fe powder was placed to synthesize the gas to produce the AMS target, iron carbide. The target material was heated at 550 °C for several hours. The weight of the resulting carbon was calculated from the internal pressure of the reaction vessel (Yokoyama et al., 2010).

Samples obtained after the graphitization process contain between 30 and 200 μg of carbon. Generally, ≤1.0 mg of carbon is used in AMS radiocarbon measurements, but in recent years it has become possible to measure very small samples (i.e., tens of micrograms of carbon; Yokoyama et al., 2010, 2022). For trace amount analysis, the reference material must be adjusted according to carbon content of the sample. For blank correction, ^{14}C-free Glycine (Wako Pure Chemical Industries, Ltd., JIS Special Grade; 0.04 ± 0.11 percent modern carbon (pMC)) is used for each measurement (Yamane et al., 2019).

The graphitized samples were placed in an aluminum holder, pressed together with silver powder, and packed in cathodes and discs (Yokoyama et al., 2010; Yamane et al., 2019). The disk-packed samples were measured with a single-stage accelerator at the Atmosphere and Ocean Research Institute, University of Tokyo (Yokoyama, 2019). A total of nine pollen samples were measured. For comparison, the residual waste material (i.e., the material rejected in the sorting process) of three samples were also measured.

4. Result and discussion

4.1. Extraction of fossil pollen

Fig. 3 illustrates the regions where fossil pollen was successfully extracted from one of the Site MOT-15-2 cores (1.7–1.72 m composite depth; mcd). First, region P1 was defined by comparing channels FL2 and FL5 to exclude particles exhibiting low fluorescence intensity, which are typically composed of lithic material and organic fragments (Fig. 3a). Region P2 contains ~90% of the grains in region P1 and was defined based on high FSC (large particle size) and high fluorescence intensity in channel FL2. Region P2 was retained as the sorted sample, with the rest designated as residual waste material. Examination of the sorted sample indicates it is comprised of ~99% fossil pollen with little to no damage caused by the sorting process (Fig. 3d). Prior to sorting, the sample contained a high concentration of impurities such as millimeter-scale lithic fragments and charcoal (Fig. 3c).

Table 1
Property of pollen grains, waste (non-pollen) material and results of radiocarbon measurement for MOT-15-2. The calibrated 95.4% Highest posterior density (HPD) was determined using MatCal (Lougheed and Obrochta, 2016) and the IntCal20 calibration curve (Reimer et al., 2020).

Lab ID	sample	top (mcd)	bottom (mcd)	14C age (BP)	14C err	CO2 extraction	carbon content (% C)	sample amount (μg C)	sediments (mg)	sample weight (mg)	total event number	grain number	pollen concentration (%)	95.4 HPD intervals (cal BP)	
YAUT-076114	pollen	0.165	0.185	1439	59	EA	30.4	46	26.61	0.19	680642	9986	1.47	1416–1270	
YAUT-076115	pollen	0.63	0.65	2187	71	EA	29.2	43	27.82	0.21	2555774	110388	4.32	2239–2038	2031–2002
YAUT-075623	pollen	1.17	1.19	2246	44	EA	29.1	95	24.11	0.12	4805676	249550	5.19	2345–2284	2279–2147
YAUT-056328	pollen	1.7	1.72	2674	43	Furnace	–	106	11.88	1.03	3379288	77028	2.28	2860–2738	
YAUT-065117	pollen	2.26	2.28	3708	74	EA	26	30	9.827	0.19	3152708	17074	0.54	4255–3840	4290–4268
YAUT-065119	waste material	2.26	2.28	5331	138	EA	19.8	40	9.827	2.45	–	–	–	6398–5380	5825–5754
YAUT-076122	pollen	2.395	2.41	4110	62	EA	16.9	34	27.81	0.28	384737	13451	3.50	4828–4512	4484–4443
YAUT-063511	pollen	3.165	3.185	4824	60	Furnace	–	165	9.699	0.97	2976425	92145	3.10	5660–5449	5382–5329
YAUT-063509	waste material	3.165	3.185	5390	62	Furnace	–	110	9.699	0.69	–	–	–	6295–6103	6090–6001
YAUT-065127	pollen	3.405	3.425	6018	233	EA	2.76	33	9.889	1.68	3242461	21187	0.65	7421–7378	7363–6369
YAUT-065129	waste material	3.405	3.425	9714	108	EA	2.52	39	9.889	2.83	–	–	–	11323–10717	11387–11382
YAUT-076123	pollen	3.54	3.56	7962	102	EA	30.6	28	28.3	0.12	356663	11505	3.23	9089–9050	9032–8544

Sheath liquid containing particles was detected by the laser and then sprayed from a nozzle at a rate of ~1000 particles/second. Particles determined to be fossil pollen were automatically transferred to the sample reservoir by applying water pressure. Efficient extraction of fossil pollen was archived by sufficient concentration of the sample solution to collect 10,000 to 100,000 fossil pollen from each sample weighing approximately 10–30 g.

4.2. Efficiency of purification and sorting

The fossil pollen extracted from region P2 are primarily produced by pine trees and generally exceed 100 μm, which is too large to extract using traditional sorting methods. This is consistent with previous studies indicating that pollen deposited in Lake Motosu are comprised of 70% pine tree genera (*Pinus*, *Tsuga*, *Pisea*, *Abies*) (YIES, 2004). Previously, the high ratio of large pollen grains would have further complicated extraction and concentration because the scarcity of smaller grains, but the method described here allows efficient ^{14}C measurement of pollen, even in areas with a large number of coniferous trees. Between ~30 and 165 μg of carbon was extracted from 2-cm samples.

Fossil pollen exhibit strong fluorescence at the wavelengths detected by channels FL2 and FL5, which is believed to reflect the thickness and surface structure of the grains. Previous studies have suggested the possibility of using fluorescence to identify different pollen types (e.g., Tennant et al., 2013; Yamada et al., 2021). If the separation of fossil pollen of a single species can be achieved, it will allow even more reliable dating.

The extracted fossil pollen contained between 16.9 and 30.6 wt% carbon (Table 1). Previous studies reported that pine pollen contain ~55 wt% carbon (Ujiié et al., 2003). One possibility for this discrepancy is that the mass of the silver cups may have been attributed to pollen. In this study, ultra-pure water and pollen were taken in silver cups and the weight after drying was determined. Since the pollen mass is very low, errors in weight may have been introduced.

4.3. ^{14}C dating of pollen

The ^{14}C ages of the fossil pollen and residual waste material from the cell sorter were verified by comparing them to the ^{14}C ages of stratigraphically proximal leaf macrofossils in Site MOT-15-2 cores (Fig. 4, Table 1). At a depth of 1.7 mcd, the age of fossil pollen was 2674 ± 43 BP (YAUT-056328). Fossil leaves were 2770 ± 73 BP (Obrochta et al., 2018), indicating that the fossil pollen and leaves agree within error, while bulk sediment is 300–350 years older (2965 ± 30 BP). Thus, the pollen extraction method established in this study can be applied to lake sediments. At a depth of 3.04 mcd there is an approximate 4000 year offset between the ^{14}C ages of fossil pollen and the waste material (YAUT-063511 and YAUT-063509), illustrating the profound effect of old carbon on bulk sediment. Both the ^{14}C ages of bulk sediments and fossil pollen were systematically older at 0.63 mcd (YAUT-076115), possibly due to minor reworking. Measuring both fossil pollen and bulk sediment helps with interpretation of the dating results at this depth, improving the accuracy of overall ^{14}C dating chronology. The 0.63 mcd sample is excluded from subsequent discussion.

Some of the pioneering ^{14}C dating of fossil pollen agreed poorly with large fossils such as leaves (e.g., Kasai et al., 2021; Zimmerman et al., 2019). Possible reasons for such discrepancies include lack of purity of the pollen and/or modern CO_2 contamination during the pre-treatment process. However, our results indicate that when >10,000 fossil pollen grains (corresponding to 30–50 μg C) are used, accurate ^{14}C dating is possible with appropriate pretreatment crosscheck by ^{14}C measurements of bulk sediment.

4.4. Implications for lake Motosu carbon reservoir age

The increased temporal resolution of terrestrial radiocarbon dates allows us to better understand the variability in the reservoir age (R) of Lake Motosu. In particular, changes in R are revealed to be more gradual than that suggested in the previous study (Fig. 5, Table 2). R is calculated as the difference between the pollen ^{14}C ages and the ^{14}C age of bulk sediments. This assumes that the old carbon is mainly stored as dissolved inorganic carbon in the lake water. C/N ratios obtained during dating suggest a primarily aquatic source of organic matter, though some contribution from terrestrial sources is also indicated. Six pollen ^{14}C ages were used to calculate variations in R, doubling the number of stratigraphic levels relative to previous studies, as terrestrial

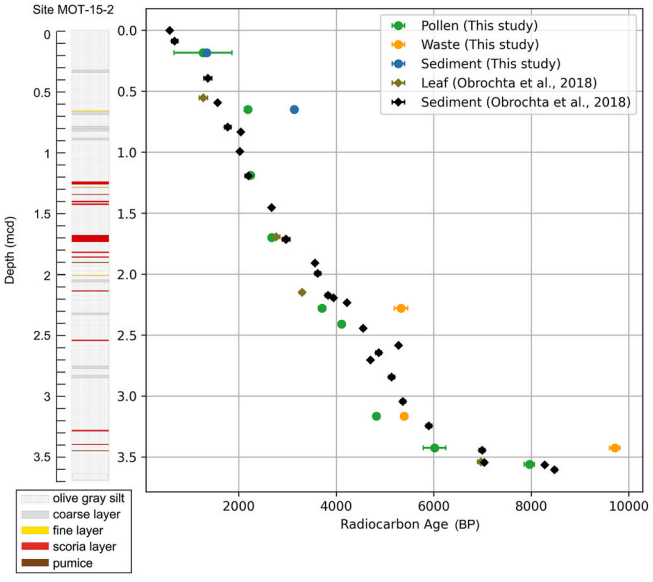

Fig. 4. Schematic columnar section of MOT-15-2 sediments and the results of radiocarbon age. The stratigraphic column shows silt (dot) and scoria layers (red). Radiocarbon age-depth plot of the fossil pollen (green circles) from nine samples, waste material (orange circles), leaves (dark green squares), and bulk sediments (black squares).

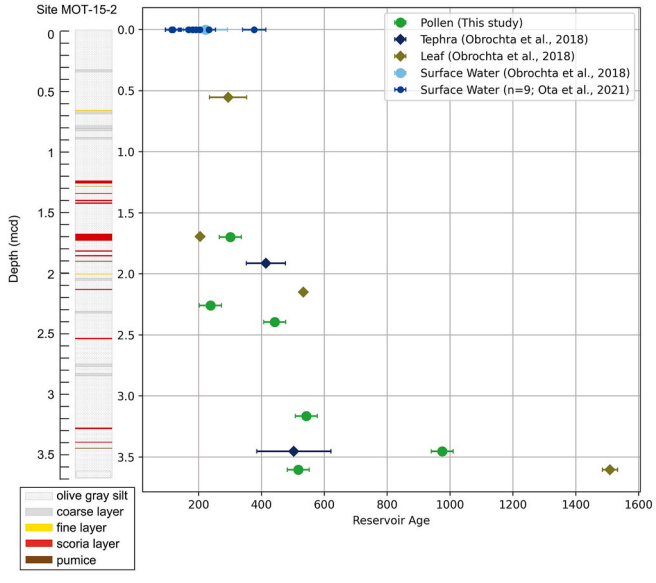

Fig. 5. Calculation of temporal changes in carbon reservoir age using bulk sediments results corresponding to tephra layers and pollen results. The R between core top to 1.715 mcd is around 300 years. R linearly increased from 414 ± 62 to 503 ± 118 between the Kg (1.915 mcd) and K-Ah (3.455 mcd) tephras, respectively. Prior to deposition of the K-Ah tephra, the carbon reservoir age was large, 1509 ± 24 at 3.605 mcd.

Table 2
Carbon reservoir age offsets of MOT-15-2.

top (mcd)	material	reservoir age offsets	error	
0.001	lake water	222	70	Obrochta et al. (2018)
0.555	Leaf	294	59	Obrochta et al. (2018)
1.695	Leaf	205	5	Obrochta et al. (2018)
1.7	Pollen	301	35	This study
1.915	Kg tephra	414	62	Obrochta et al. (2018)
2.15	Leaf	533	6	Obrochta et al. (2018)
2.26	Pollen	238	33	This study
2.395	Pollen	442	22	This study
3.165	Pollen	542	12	This study
3.405	Pollen	975	175	This study
3.455	K-Ah tephra	503	118	Obrochta et al. (2018)
3.54	Pollen	517	54	This study
3.605	Leaf	1509	24	Obrochta et al. (2018)

radiocarbon ages are now available where leaf fossils were not found.

The modern R of Lake Motosu is 222 ± 70 years and was larger in the past (Obrochta et al., 2018; Ota et al., 2021). Prior to ~8000 BP, R was initially large at 800–1000 years before gradually decreasing to 700–300 years from ~7000 BP to present. Radiocarbon ages of DIC in surface water (i.e., R) is around 115–377 years from September 2018 to April 2019, which suggests the age of the surface sediments should primarily reflect the ^{14}C ages of source water (Ota et al., 2021). In upland areas, precipitation variability has been suggested to be an important factor in changes in carbon reservoir effect, with variations of several hundred years occurring in Central Asia (Zhou et al., 2015). Although it cannot be simply compared with Lake Motosu due to the difference in depositional environment, the hydroclimate environment may be influencing the R of lake water. In the future, additional R data at higher temporal resolution may reveal paleoclimatic changes around Mt. Fuji.

5. Conclusions

The methodology introduced here makes collection of large (>100 μm) fossil pollen grains possible through systematic combination of physical and chemical pretreatment prior to flow cytometry purification. The radiocarbon ages of the fossil pollen extracted this way are consistent with leaf fossils obtained from identical or proximal depths in the same sediment core. Since pollen is more resistant and more common than leaves in lake sediment, applying this method will greatly improve the chronologies of lakes that lack clear, annual layers and contribute to improved spatio-temporal resolution in paleoclimate research.

Comparison of fossil pollen with bulk sediments has revealed variations in R over the past 8000 years at Lake Motosu, Japan. The magnitude of the carbon reservoir effect is not constant and decreases towards the present. Variations in carbon reservoir effect reflect the environment at the time of deposition and are, therefore, worth considering as proxies for hydroclimate and/or depositional environments through simultaneous measurements with fossil pollen.

CRediT authorship contribution statement

Kosuke Ota: Writing – original draft, Methodology, Investigation, Formal analysis, Conceptualization. **Yusuke Yokoyama:** Writing – review & editing, Supervision, Resources, Project administration, Investigation, Funding acquisition, Conceptualization. **Yosuke Miyairi:** Writing – review & editing, Methodology. **Stephen P. Obrochta:** Writing – review & editing, Software. **Shinya Yamamoto:** Writing – review & editing. **A. Hubert-Ferrari:** Writing – review & editing. **V.M. A. Heyvaert:** Writing – review & editing. **Marc De Batist:** Writing – review & editing. **Osamu Fujiwara:** Writing – review & editing.

Declaration of competing interest

The authors declare that they have no known competing financial interests or personal relationships that could have appeared to influence the work reported in this paper.

Data availability

The data that has been used is confidential.

Acknowledgements

We thank to Dr. Shigeru Suzuki for teaching physical and chemical pre-treatment of fossil pollen. We thank to Drs. Takahiro Aze and Chikako Sawada for helping radiocarbon measurement about the AMS at AORI. We thank to Dr. B. Behrens for improving manuscript. We would like to express my gratitude to Japan Science and Technology Agency (JST) SPRING, (JPMJSP 2108) for their financial support. Core MOT-15-2 was obtained during QuakeRecNankai project supported by the Belgian Science Policy Office (BELSPO BRAIN-be BR/121/A2). This work was partly supported by JST, CREST Grant JPMJCR23J6, Japan and a grant from the Japan Society for the Promotion of Science (JSPS) KAKENHI 16K05571 and 23KK0013.

References

Bertrand, S., Araneda, A., Vargas, P., Jana, P., Fagel, N., Urrutia, R., 2012. Using the N/C ratio to correct bulk radiocarbon ages from lake sediments: insights from Chilean Patagonia. Quat. Geochronol. 12, 23–29. https://doi.org/10.1016/j.quageo.2012.06.003.

Brown, T.A., Nelson, D.E., Mathewes, R.W., Vogel, J.S., Southon, J.R., 1989. Radiocarbon dating of pollen by accelerator mass spectrometry. Quat. Res. 32, 205–212. https://doi.org/10.1016/0033-5894(89)90076-8.

Fletcher, W.J., Zielhofer, C., Mischke, S., Bryant, C., Xu, X., Fink, D., 2017. AMS radiocarbon dating of pollen concentrates in a karstic lake system. Quat. Geochronol. 39, 112–123. https://doi.org/10.1016/j.quageo.2017.02.006.

Geyh, M.A., Schotterer, U., Grosjean, M., 1997. Temporal changes of the 14C reservoir effect in lakes. Radiocarbon 40, 921–931. https://doi.org/10.1017/S0033822200018890.

Hamada, H., Daiki, K., Oyagi, H., 2012. Investigation of seasonal change of water temperature and water quality and water balance on lake motosu-ko. Bull. Fac. Educ. Chiba Univ. 60, 459–468.

Hou, J., D'Andrea, W.J., Liu, Z., 2012. The influence of 14C reservoir age on interpretation of paleolimnological records from the Tibetan Plateau. Quat. Sci. Rev. 48, 67–79. https://doi.org/10.1016/j.quascirev.2012.06.008.

Howarth, J.D., Fitzsimons, S.J., Jacobsen, G.E., Vandergoes, M.J., Norris, R.J., 2013. Identifying a reliable target fraction for radiocarbon dating sedimentary records from lakes. Quat. Geochronol. 17, 68–80. https://doi.org/10.1016/j.quageo.2013.02.001.

Hua, Q., Jacobsen, G.E., Zoppi, U., Lawson, E.M., Williams, A.A., Smith, A.M., McGann, M.J., 2001. Progress in radiocarbon target preparation at the antares AMS centre. Radiocarbon 43, 275–282. https://doi.org/10.1017/S003382220003811X.

Kasai, Y., Leipe, C., Saito, M., Kitagawa, H., Lauterbach, S., Brauer, A., Tarasov, P.E., Goslar, T., Arai, F., Sakuma, S., 2021. Breakthrough in purification of fossil pollen for dating of sediments by a new large-particle on-chip sorter. Sci. Adv. 7, eabe7327 https://doi.org/10.1126/sciadv.abe7327.

Koshimizu, S., Uchiyama, T., Yamamoto, G., 2007. Volcanic history of Mt.Fuji recorded in borehole cores from Fuji Five Lakes surrounding Mt. Fuji. Fuji Volcano 365–374.

Lougheed, B., Obrochta, S., 2016. MatCal: open source bayesian ^{14}C age calibration in matlab. J. Open Res. Software 4, e42. https://doi.org/10.5334/jors.130.

Miyaji, N., 1988. History of younger Fuji volcano. J. Geol. Soc. Jpn. 94, 433–452. https://doi.org/10.5575/geosoc.94.433.

Morita, Y., 2012. A guide to pollen analysis and microscopy, with an aim to improve its working efficiency. Jpn. Assoc. Hist. Bot. 21, 73–84.

Nakamura, A., Yokoyama, Y., Maemoku, H., Yagi, H., Okamura, M., Matsuoka, H., Miyake, N., Osada, T., Adhikari, D.P., Dangol, V., Ikehara, M., Matsuzaki, H., 2016. Weak Monsoon event at 4.2 ka recorded in sediment from Lake Rara, Himalayas. Quat. Int. 397, 349–359. https://doi.org/10.1016/j.quaint.2015.05.053.

Obrochta, S.P., Yokoyama, Y., Yoshimoto, M., Yamamoto, S., Miyairi, Y., Nagano, G., Nakamura, A., Tsunematsu, K., Lamair, L., Hubert-Ferrari, A., Lougheed, B.C., Hokanishi, A., Yasuda, A., Heyvaert, V.M.A., De Batist, M., Fujiwara, O., 2018. Mt. Fuji Holocene eruption history reconstructed from proximal lake sediments and high-density radiocarbon dating. Quat. Sci. Rev. 200, 395–405. https://doi.org/10.1016/j.quascirev.2018.09.001.

Omori, T., Yamada, K., Kitaba, I., Hori, T., Nakagawa, T., 2023. Reliable radiocarbon dating of fossil pollen grains: it is truly possible. Quat. Geochronol. 77, 101456 https://doi.org/10.1016/j.quageo.2023.101456.

Ota, K., Yokoyama, Y., Miyairi, Y., Yamamoto, S., Miyajima, T., 2021. Lake water dissolved inorganic carbon dynamics revealed from monthly measurements of radiocarbon in the Fuji Five Lakes, Japan. Elementa. Sci. Anthr. 9, 00149 https://doi.org/10.1525/elementa.2020.00149.

Ota, K., Yokoyama, Y., Miyairi, Y., Yamamoto, S., Wang, Y., Miyajima, T., 2023. Monthly measurements of water dissolved inorganic radiocarbon in Lake Kawaguchi for three years indicating seasonal precipitation-groundwater variations. Nucl. Instrum. Methods Phys. Res. Sect. B Beam Interact. Mater. Atoms 538, 75–80. https://doi.org/10.1016/j.nimb.2023.02.021.

Philippsen, B., 2013. The freshwater reservoir effect in radiocarbon dating. Herit. Sci. 1, 24. https://doi.org/10.1186/2050-7445-1-24.

Reimer, P.J., Austin, W.E.N., Bard, E., Bayliss, A., Blackwell, P.G., Ramsey, C.B., Butzin, M., Cheng, H., Edwards, R.L., Friedrich, M., Grootes, P.M., Guilderson, T.P., Hajdas, I., Heaton, T.J., Hogg, A.G., Hughen, K.A., Kromer, B., Manning, S.W., Muscheler, R., Palmer, J.G., Pearson, C., Plicht, J. van der, Reimer, R.W., Richards, D.A., Scott, E.M., Southon, J.R., Turney, C.S.M., Wacker, L., Adolphi, F., Büntgen, U., Capano, M., Fahrni, S.M., Fogtmann-Schulz, A., Friedrich, R., Köhler, P., Kudsk, S., Miyake, F., Olsen, J., Reinig, F., Sakamoto, M., Sookdeo, A., Talamo, S., 2020. The IntCal20 northern hemisphere radiocarbon age calibration curve (0–55 cal kBP). Radiocarbon 62, 725–757. https://doi.org/10.1017/RDC.2020.41.

Shah, S.R., Pearson, A., 2007. Ultra-microscale (5–25 μg C) analysis of individual lipids by 14C AMS: assessment and correction for sample processing blanks. Radiocarbon 49, 69–82. https://doi.org/10.1017/S0033822200041904.

Steinhoff, C., Pickarski, N., Litt, T., Hajdas, I., Welte, C., Wurst, P., Kühne, D., Dolf, A., Germer, M., Kallmeyer, J., 2022. New approach to separate and date small spores and pollen from Lake sediments in semi-arid climates. Radiocarbon 1–17. https://doi.org/10.1017/RDC.2022.34.

Takada, A., Mannen, K., Yamamoto, T., 2013. Fuji and Hakone volcanoes: typical stratovol- canoes in Japan, IAVCEI 2013 field trip guide. Bull. Geol. Surv. Jpn. 58, 1–26.

Takada, A., Yamamoto, T., Isizuka, Y., Nakano, S., 2016. Fujisan: Geological Maps of Volcanoes. Geological Survey of Japan, AIST.

Tani, S., Kitagawa, H., Hong, W., Park, J.H., Sung, K.S., Park, G., 2013. Age determination of the kawagodaira volcanic eruption in Japan by 14C wiggle-matching. Radiocarbon 55, 748–752. https://doi.org/10.1017/S0033822200057908.

Tennant, R.K., Jones, R.T., Brock, F., Cook, C., Turney, C.S.M., Love, J., Lee, R., 2013. A new flow cytometry method enabling rapid purification of fossil pollen from terrestrial sediments for AMS radiocarbon dating: cytometric pollen purification for ^{14}C dating. J. Quat. Sci. 28, 229–236. https://doi.org/10.1002/jqs.2606.

Tunno, I., Zimmerman, S.R.H., Brown, T.A., Hassel, C.A., 2021. An improved method for extracting, sorting, and AMS dating of pollen concentrates from Lake sediment. Front. Ecol. Evol. 9.

Ujiié, Y., Arata, Y., Sugawara, M., 2003. Heating experiments on *Pinus* pollen grains and its relation to petroleum genesis. Geochem. J. 37, 367–376. https://doi.org/10.2343/geochemj.37.367.

Yamada, K., Omori, T., Kitaba, I., Hori, T., Nakagawa, T., 2021. Extraction method for fossil pollen grains using a cell sorter suitable for routine 14C dating. Quat. Sci. Rev. 272, 107236 https://doi.org/10.1016/j.quascirev.2021.107236.

Yamamoto, S., Kametani, N., Yoshimoto, M., Miyairi, Y., Yokoyama, Y., 2023. Eruptive history of Mt. Fuji over the past 8000 years based on integrated records of lacustrine and terrestrial tephra sequences and radiocarbon dating. Quat. Sci. Adv. 12, 100091 https://doi.org/10.1016/j.qsa.2023.100091.

Yamamoto, T., Takada, A., Ishizuka, Y., Nakano, S., 2005. Chronology of the products of Fuji volcano based on new radiometoric carbon ages. Bull. Volcanol. Soc. Jpn. 50, 53–70. https://doi.org/10.18940/kazan.50.2_53.

Yamane, M., Yokoyama, Y., Hirabayashi, S., Miyairi, Y., Ohkouchi, N., Aze, T., 2019. Small- to ultra-small-scale radiocarbon measurements using newly installed single-stage AMS at the University of Tokyo. Nucl. Instrum. Methods Phys. Res. Sect. B Beam Interact. Mater. Atoms 455, 238–243. https://doi.org/10.1016/j.nimb.2019.01.035.

YIES, 2004. Yamanashi Institute of environmental scienses report. Yamanashi Inst. Environ. Sciense Rep. 8.

Yokoyama, Y., 2019. A single stage accelerator mass spectrometry at the Atmosphere and Ocean Research Institute, the university of Tokyo. Nucl. Instrum. Methods Phys. Res. Sect. B Beam Interact. Mater. Atoms 455, 311–316.

Yokoyama, Y., Koizumi, M., Matsuzaki, H., Miyairi, Y., Ohkouchi, N., 2010. Developing ultra small-scale radiocarbon sample measurement at the university of Tokyo. Radiocarbon 52, 310–318. https://doi.org/10.1017/S0033822200045355.

Yokoyama, Y., Miyairi, Y., Aze, T., Sawada, C., Ando, Y., Izawa, S., Ueno, Y., Hirabayashi, S., Fukuyo, N., Ota, K., Shimizu, Y., Zeng, Y., Lan, H., Tsuneoka, R., Ando, K., Nemoto, K., Obrochta, S., Behrens, B., Tam, E., Leggett, K., Rzeszewicz, J., Huang, Z., Kondo, R., Nagata, T., 2022. Efficient radiocarbon measurements on marine and terrestrial samples with single stage accelerator mass spectrometry at the Atmosphere and Ocean Research Institute. University of Tokyo. Nucl. Instrum. Methods Phys. Res. Sect. B Beam Interact. Mater. At. 532, 62–67. https://doi.org/10.1016/j.nimb.2022.10.006.

Zhang, Q., Liu, X., Li, H., 2021. Impact of hydrological conditions on the radiocarbon reservoir effect in lake sediment 14C dating: the case of Kusai Lake on the northern Qinghai-Tibet Plateau. Quat. Geochronol. 62, 101149 https://doi.org/10.1016/j.quageo.2020.101149.

Zhou, A., He, Y., Wu, D., Zhang, X., Zhang, C., Liu, Z., Yu, J., 2015. Changes in the radiocarbon reservoir age in Lake xingyun, Southwestern China during the holocene. PLoS One 10, e0121532. https://doi.org/10.1371/journal.pone.0121532.

Zimmerman, S.R.H., Brown, T.A., Hassel, C., Heck, J., 2019. Testing pollen sorted by flow cytometry as the basis for high-resolution lacustrine chronologies. Radiocarbon 61, 359–374. https://doi.org/10.1017/RDC.2018.89.